Zebrafish *mbnl* mutants model molecular and physical phenotypes of human *MBNL* loss of function disorders

Melissa N. Hinman[1], Jared I. Richardson[4,6], Rose A. Sockol[1], Eliza D Aronson[1], Sarah J. Stednitz[2], Katrina N. Murray[3], J. Andrew Berglund[4,6], and Karen Guillemin[1,5*]

[1]Institute of Molecular Biology, [2]Institute of Neuroscience, [3]Zebrafish International Resource Center, University of Oregon, Eugene, Oregon, [4]RNA Institute, State University of New York at Albany, Albany, New York, [5]Humans and the Microbiome Program, CIFAR, Toronto, Ontario M5G 1Z8, Canada, [6]Center for NeuroGenetics, University of Florida, Gainesville, Florida

*Corresponding author
Corresponding author email address: kguillem@uoregon.edu
Corresponding author ORCID identifier: https://orcid.org/0000-0001-6004-9955

Key words: myotonic dystrophy, Fuchs endothelial corneal dystrophy, zebrafish disease models, MBNL1, MBNL2, MBNL3

Summary Statement

Zebrafish *mbnl* mutants that were generated to model myotonic dystrophy and Fuchs endothelial corneal dystrophy exhibited disease-relevant phenotypes including alternative splicing changes, decreased body size, and impaired movement.

Abstract

The muscleblind RNA binding proteins (MBNL1, MBNL2, and MBNL3) are highly conserved across vertebrate species and are important regulators of alternative splicing and other aspects of RNA metabolism. Loss of MBNL protein function through sequestration by CUG or CCUG RNA repeats is partially responsible for the phenotypes of two important human genetic disorders, myotonic dystrophy (DM) and Fuchs endothelial corneal dystrophy (FECD). We generated the first stable zebrafish (*Danio rerio*) models of *MBNL* loss of function disorders through CRISPR-based mutation of the three zebrafish *mbnl* genes. In contrast to mouse models, zebrafish double and triple homozygous *mbnl* mutants were viable to adulthood. Zebrafish *mbnl* mutants displayed many DM- and FECD-associated alternative splicing changes in disease relevant tissues. In general, *mbnl1* and *mbnl2* mutants displayed more pronounced alternative splicing defects than *mbnl3* mutants, and compound *mbnl* mutants exhibited larger splicing changes than single *mbnl* mutants. Splicing changes in zebrafish *mbnl* mutants were greatest in adult heart and skeletal muscle. Zebrafish *mbnl* mutants displayed disease relevant physical phenotypes including decreased sized and impaired movement. The high fecundity and larval optical transparency of these new zebrafish models will make them useful for studying DM- and FECD- related phenotypes and how individual Mbnl proteins contribute to them.

Introduction

The muscleblind (MBNL) family of RNA binding proteins is highly conserved in structure and function across multicellular species, and vertebrates have three family members: MBNL1, MBNL2, and MBNL3 (Oddo et al., 2016). MBNL proteins use zinc finger motifs (two pairs in the case of vertebrates) to recognize and bind to consensus YGCY sequences (where Y is a pyrimidine) in target RNAs and regulate multiple aspects of RNA metabolism, the most well-characterized of which is alternative splicing (Ashwal-Fluss et al., 2014; Batra et al., 2014; Goers et al., 2010; Grammatikakis et al., 2011; Ho et al., 2004; Rau et al., 2011; Wang et al., 2012; Warf and Berglund, 2007). In general, MBNL proteins promote exon skipping when bound to YGCY sequences in the intron upstream of an alternative exon, and promote exon inclusion when bound downstream of an alternative exon (Du et al., 2010; Goers et al., 2010; Wang et al., 2012). Regulation of alternative splicing by MBNL proteins is critical for the molecular function of many target genes. For example, MBNL proteins promote skipping of exon 5 in the *MBNL1* and *MBNL2* mRNAs by binding to highly conserved YGCY elements in the upstream intron, affecting the subcellular localization and alternative splicing regulatory activity of the resulting proteins (Gates et al., 2011; Terenzi and Ladd, 2010; Tran et al., 2011).

The regulation of RNA metabolism by MBNL proteins is crucial for the proper functioning of many body systems, as shown by the multi-systemic phenotypes in human genetic disorders that involve *MBNL* loss of function. In myotonic dystrophy (DM), expression of an expanded CTG repeat in the 3' UTR of the *DMPK* gene (DM1) or an expanded CCTG repeat in an intron of the *CNBP* gene (DM2) leads to the formation of RNA stem loop structures that contain dozens to thousands of YGCY motifs that bind and sequester MBNL proteins, preventing them from performing their normal functions (Brook et al., 1992; Fardaei et al., 2002; Fu et al., 1992; Liquori et al., 2001; Mahadevan et al., 1992; Miller et al., 2000) (Fig. 1A). DM is most well-known for its skeletal muscle phenotypes, including weakness, myotonia, atrophy, and pain. However, individuals with DM experience a wide variety of symptoms in many tissues that can be as debilitating as muscle phenotypes, including but not limited to cataracts,

75 breathing difficulties, behavioral and psychological disorders, sleep disorders, insulin
76 resistance, heart conduction abnormalities, cardiomyopathy, and alterations in the
77 motility and microbiota of the gut (Bellini et al., 2006; Hilbert et al., 2017; Tarnopolsky et
78 al., 2010; Thomas et al., 2018; Tieleman et al., 2008; Wenninger et al., 2018).
79 Misregulation of specific alternative splicing events was shown to contribute to disease-
80 related phenotypes (Thomas et al., 2018). For example, missplicing of *RYR1* and
81 *ATP2A1* contributed to altered calcium homeostasis in DM1 muscle (Kimura et al.,
82 2005; Zhao et al., 2015). Fuchs endothelial corneal dystrophy (FECD) leads to corneal
83 edema and loss of vision, and a subtype of this common disorder was recently shown to
84 be caused by an expanded CUG repeat that is expressed from an intron of the *TCF4*
85 gene. Signs of FECD were also reported in a subset of individuals with DM1 (Mootha et
86 al., 2017; Mootha et al., 2015; Wieben et al., 2017; Winkler et al., 2018). As in DM,
87 MBNL protein sequestration and missplicing were demonstrated in FECD, but how
88 MBNL loss of function contributes to the disease phenotype is not understood (Du et al.,
89 2015; Wieben et al., 2017).
90 Mouse *Mbnl* mutants greatly improved our understanding of the biological roles
91 of individual MBNL proteins and how they may contribute to human MBNL loss of
92 function disorders. Mouse *Mbnl1* is widely expressed and *Mbnl1*$^{-/-}$ mice exhibited
93 changes in alternative splicing, myotonia, myopathy, and cataracts, but did not have
94 other DM-related phenotypes such as muscle weakness, suggesting that loss of *Mbnl1*
95 function alone was not sufficient to cause all DM-related phenotypes (Kanadia et al.,
96 2003; Lee et al., 2013). *Mbnl2* expression is enriched in the brain, and *Mbnl2*$^{-/-}$ mice
97 exhibited DM-like CNS phenotypes including missplicing in the brain, abnormal sleep
98 patterns, and spatial memory deficits (Charizanis et al., 2012). Mouse *Mbnl3* is
99 expressed primarily during embryonic development and injury-induced adult skeletal
100 muscle regeneration. *Mbnl3*$^{-/-}$ mice exhibited delays in injury-induced muscle
101 regeneration, accelerated onset of age-related pathologies, and gene expression
102 changes, but displayed minimal changes in alternative splicing, suggesting that *Mbnl3*
103 played a more modest role in DM-related missplicing (Choi et al., 2016; Poulos et al.,
104 2013). Compound *Mbnl* mutant mice had more severe phenotypes than single mutant

105 mice, suggesting that Mbnl proteins had overlapping functions in mice. *Mbnl1*$^{-/-}$*;Mbnl2*$^{-/-}$
106 mice were embryonic lethal, while *Mbnl1*$^{-/-}$*;Mbnl2*$^{+/-}$ mice were viable but had severe
107 missplicing, decreased body weight, myotonia, progressive muscle weakness, and
108 reduced lifespan (Lee et al., 2013). Muscle-specific double (*Mbnl1*$^{-/-}$*; Mbnl2*$^{C/C}$*;*
109 *Mbnl3*$^{+/Y}$*; Myog-Cre*$^{+/-}$) and triple (*Mbnl1*$^{-/-}$*; Mbnl2*$^{C/C}$*; Mbnl3*$^{C/Y}$*; Myog-Cre*$^{+/-}$) mutant mice
110 were reduced in size, had dramatic and widespread alternative splicing changes,
111 muscle weakness, and most died in the neonatal period due to respiratory distress
112 (Thomas et al., 2017). Compound *Mbnl* mutant mice recapitulated many of the
113 phenotypes associated with severe forms of DM, but their utility in future experiments is
114 limited because they are difficult to generate in large numbers.
115 We sought to expand the understanding of MBNL function using another
116 vertebrate model organism, the zebrafish. Like mice, zebrafish have one ortholog of
117 each of the human *MBNL* genes (Liu et al., 2008). There are several advantages of
118 using zebrafish over mice to study Mbnl function. Zebrafish embryos develop rapidly
119 and externally, making studies of developmental phenotypes easier than in mice.
120 Zebrafish embryos are optically transparent, which allows for direct analysis of DM-
121 related phenotypes such as altered gut motility and abnormal heart rhythm. Finally,
122 zebrafish produce hundreds of embryos at once, and adults can be maintained much
123 more cheaply than mice, which enables experiments to be performed with large
124 numbers of animals and improves statistical power when studying subtle or variable
125 phenotypes. Two zebrafish models of *MBNL* loss of function disorders were generated
126 previously, but both had severe limitations. Zebrafish embryos that were injected with
127 CUG repeat RNA had subtle developmental abnormalities, but did not exhibit alternative
128 splicing changes, and the injected RNA was degraded by two days post fertilization
129 (dpf) (Todd et al., 2014). This model did not allow for the study of phenotypes beyond
130 early development, and could not distinguish between the effects of loss of individual
131 Mbnl proteins. Another model employed morpholinos, but these are also transient and
132 can have off-target effects. Morpholino-based knockdown of *mbnl2* in zebrafish
133 embryos resulted in profound morphological abnormalities that were inconsistent with

134 the much milder phenotypes observed in *Mbnl2*$^{-/-}$ mice (Charizanis et al., 2012;
135 Machuca-Tzili et al., 2011).
136 In the current study, we used CRISPR-Cas9 based mutagenesis to make
137 homozygous zebrafish *mbnl1*, *mbnl2,* and *mbnl3* loss of function mutants, which were
138 crossed to generate double (*mbnl1/mbnl2*, *mbnl2/mbnl3,* and *mbnl1/mbnl3*) and triple
139 (*mbnl1/mbnl2/mbnl3*) homozygous mutants, all of which were viable to adulthood. We
140 analyzed alternative splicing in these mutants, and found that they exhibited many of
141 the same changes that were present in human *MBNL* loss of function disorders and
142 mouse *Mbnl* mutants. These alternative splicing changes occured both in larval and
143 adult fish, but were most dramatic in adult skeletal and heart muscle. As in mice,
144 double and triple homozygous zebrafish *mbnl* mutants exhibited larger alternative
145 splicing changes than single mutants and had decreased body size. *mbnl* mutants also
146 had decreased swim test performance. Thus, zebrafish *mbnl* mutants had molecular
147 and physical phenotypes consistent with those present in human *MBNL* loss of function
148 disorders, and are a powerful new vertebrate model for studies of *MBNL* function.

149 **Results**

150 **Generation of a comprehensive set of zebrafish *mbnl* mutants**

151 To create stable zebrafish models of *mbnl* loss of function disorders, we used
152 CRISPR/Cas9 technology and mutated zebrafish *mbnl1*, *mbnl2,* and *mbnl3*. We
153 targeted constitutively included exons in each zebrafish *mbnl* gene (Liu et al., 2008),
154 and established two independent *mbnl1* mutant lines ($1^{A/A}$ and $1^{B/B}$), one *mbnl2* mutant
155 line ($2^{A/A}$), and three independent *mbnl3* mutant lines ($3^{A/A}$, $3^{B/B}$, $3^{C/C}$) (Fig. 1B, Table
156 S1, and Table S2). The *mbnl* mutations were predicted to result in a frameshift leading
157 to a premature termination codon (1^{A}, 2^{A}, 3^{A}, and 3^{B}), insertion of an early stop codon
158 (3^{C}), or loss of the start codon leading to usage of a downstream out-of-frame start
159 codon (1^{B}) (Fig. 1B and Table S2). Each mutation was also predicted to result in loss of
160 function of one or more of the zinc fingers that are important for RNA binding (Fig. 1B)
161 (Grammatikakis et al., 2011). Homozygous larval mutants exhibited decreased ($2^{A/A}$,
162 $3^{A/A}$, and $3^{B/B}$) or unchanged ($1^{A/A}$, $1^{B/B}$, and $3^{C/C}$) levels of the mRNA expressed from

163 the mutated gene, with minimal effect on the expression of the other *mbnl* family
164 members (Fig. S1).
165 All homozygous *mbnl1, mbnl2,* and *mbnl3* mutants survived to adulthood in
166 roughly Mendelian ratios (Table S3), were fertile, and did not exhibit the dramatic
167 morphological phenotypes that were previously observed in *mbnl2* morpholino-injected
168 larvae (Machuca-Tzili et al., 2011). We crossed single *mbnl* mutant fish to generate
169 double *mbnl* mutants ($1^{B/B};2^{A/A}$, $1^{B/B};3^{C/C}$, and $2^{A/A};3^{C/C}$). All double *mbnl* mutants were
170 also viable to adulthood and fertile (Table S3). This contrasted with mouse models, in
171 which $mbnl^{-/-};mbnl2^{-/-}$ mutants were embryonic lethal, and to our knowledge represented
172 the first time that *mbnl1/mbnl3* and *mbnl2/mbnl3* double homozygous mutant animals
173 were generated (Lee et al., 2013). We further crossed double homozygous animals to
174 generate triple homozygous mutants ($1^{B/B};2^{A/A};3^{C/C}$). Surprisingly, these fish were viable
175 to adulthood, albeit in lower than expected numbers (Table S3), but they were unable to
176 produce embryos except through *in vitro* fertilization. In summary, we created the first
177 complete panel of vertebrate *mbnl1, mbnl2,* and *mbnl3* single, double, and triple
178 homozygous mutants for studying the functions of Mbnl proteins.

179 **Larval zebrafish *mbnl* mutants displayed disease-associated changes in**
180 **alternative splicing**

181 We first asked whether zebrafish *mbnl* mutants modeled the alternative splicing
182 changes observed in humans with DM and FECD and in mouse *Mbnl* mutants. Our
183 initial studies used the extensively characterized suppression of *mbnl1* exon 5 and
184 *mbnl2* exon 5 inclusion by Mbnl proteins as a model system (Gates et al., 2011). The
185 intronic sequence immediately upstream of exon 5, which contains putative YGCY Mbnl
186 protein binding sites, is highly conserved between human and zebrafish, suggesting
187 functional importance (Fig. S2).
188 We harvested total RNA from larval zebrafish and analyzed exon inclusion
189 through RT-PCR analysis. Inclusion of both *mbnl1* exon 5 and *mbnl2* exon 5 was
190 elevated in zebrafish *mbnl* mutants (Fig. 2A,B). The effect was very modest in single
191 homozygous *mbnl* mutants, with only one of two *mbnl1* homozygous mutants showing
192 slightly increased inclusion of both *mbnl1* exon 5 and *mbnl2* exon 5, and $2^{A/A}$ mutants

193 displaying increased inclusion of *mbnl2* exon 5 only (Fig. 2A,B). Exon 5 inclusion was
194 elevated in double homozygous *mbnl* mutants above that in single homozygous
195 mutants, with the highest level of exon inclusion observed in $1^{B/B};2^{A/A}$ mutants (Fig.
196 2A,B). This suggested that zebrafish Mbnl proteins had overlapping functions in
197 splicing regulation, similar to findings in mice (Lee et al., 2013; Thomas et al., 2017).
198 *mbnl3* contributed minimally to autoregulation of *mbnl* splicing in larval fish, as none of
199 the three *mbnl3* single mutants showed elevated *mbnl1* or *mbnl2* exon 5 inclusion, and
200 $1^{B/B};2^{A/A};3^{C/C}$ mutants did not show increased exon 5 inclusion compared to $1^{B/B};2^{A/A}$
201 mutants (Fig. 2A,B). This was consistent with mouse data, in which *mbnl3* contributed
202 minimally to splicing regulation (Choi et al., 2016; Poulos et al., 2013).

203 **Adult zebrafish *mbnl* mutant skeletal muscle showed robust alternative splicing**
204 **changes**

205 A well-characterized pattern in DM is a tendency to switch from the production of
206 adult-specific RNA isoforms to the production of isoforms that are normally found in
207 development (Kalsotra et al., 2008; Lin et al., 2006). Therefore, the magnitude of DM-
208 associated splicing changes tends to be larger in adult tissues than in embryos. We
209 asked whether this was also the case in zebrafish *mbnl* mutants, focusing on skeletal
210 muscle because it is one of the most severely affected tissues in DM. The mRNA levels
211 of *mbnl1, mbnl2*, and *mbnl3* were all higher in adult skeletal muscle than in whole larvae
212 (Fig. S3). The splicing patterns of *mbnl1* and *mbnl2* exon 5 changed much more
213 dramatically in adult *mbnl* mutant skeletal muscle than in whole larvae, from
214 predominant exon skipping in WT fish to predominant inclusion in $1^{B/B};2^{A/A}$ mutants (Fig.
215 2C,D). In mouse and DM patient tissues, some regulated exons were much more
216 sensitive than others to changes in overall levels of free MBNL proteins (Wagner et al.,
217 2016). It appears that zebrafish also followed this pattern, as in skeletal muscle *mbnl1*
218 mutation alone was sufficient to increase *mbnl1* exon 5 inclusion, whereas loss of
219 function of both *mbnl1* and *mbnl2* was required to increase *mbnl2* exon 5 inclusion (Fig.
220 2C,D). *mbnl3* played a small role in *mbnl* splicing autoregulation in skeletal muscle, as
221 $1^{B/B};2^{A/A};3^{C/C}$ mutants showed slightly elevated *mbnl2* exon 5 inclusion compared to
222 $1^{B/B};2^{A/A}$ mutants (Fig. 2D).

223 **Alternative splicing changes occurred across tissues in zebrafish *mbnl* mutants**

224 We next asked whether adult zebrafish *mbnl* mutants exhibited alternative
225 splicing changes in other tissues relevant to DM and FECD pathology. Zebrafish *mbnl1,*
226 *mbnl2,* and *mbnl3* mRNAs were all expressed broadly across tissues, with the highest
227 *mbnl* mRNA levels in skeletal muscle and brain (Fig. S3). Splicing patterns for both
228 *mbnl1* exon 5 and *mbnl2* exon 5 in the heart were very similar to those in skeletal
229 muscle (Figs 2C,D and 3A,B). The brain and cornea exhibited *mbnl* splicing patterns
230 quite similar to one another, but the magnitude of splicing changes between WT and
231 mutants was slightly lower than those observed in muscle (Fig. 3C,D,E,F). *mbnl*
232 splicing changes in the intestine were small in magnitude, and appeared to be driven
233 primarily by *mbnl1* mutation (Fig. 3G,H). Therefore, zebrafish *mbnl* mutants
234 recapitulated alternative splicing changes in disease relevant tissues.

235 **Misregulation of alternative splicing was widespread in zebrafish *mbnl* mutants**

236 We expanded our analysis to determine whether our findings related to
237 misregulation of *mbnl1* exon5 and *mbnl2* exon 5 alternative splicing in *mbnl* mutant fish
238 applied more broadly to other disease-associated missplicing events. We investigated
239 five additional exons that were conserved between human and zebrafish, two of which
240 exhibited increased inclusion in human *MBNL* loss of function disorders and/or mouse
241 models (*ank3b* exon 36 and *tpd52l2b* exon 4) and three of which exhibited decreased
242 inclusion (*atp2a1l* exon 24*, ryr1b* exon 72*,* and *csnk1da* exon 9) (Bachinski et al., 2014;
243 Freyermuth et al., 2016; Goodwin et al., 2015; Hino et al., 2007; Kimura et al., 2005).
244 Four showed splicing changes in the same direction as that observed in human *MBNL*
245 loss of function disorders and/or mouse models, while one, *csnk1da*, had a splicing
246 change in the opposite direction (Fig. 4). We noticed similarities between regulation of
247 these splicing events and auto-regulation of *mbnl1* exon 5 and *mbnl2* exon 5 inclusion.
248 For example, in all cases $1^{B/B};2^{A/A}$ mutants showed larger changes in exon inclusion
249 compared to WT than either of the other two double homozygous mutants, suggesting
250 that *mbnl1* and *mbnl2* played the largest roles in alternative splicing regulation (Fig. 4).
251 *mbnl3* appeared to play a lesser role in the regulation of these splicing events, as none
252 of the three single homozygous *mbnl3* mutants showed significant changes in inclusion

253 of any of the exons tested, and triple homozygous *mbnl* mutants did not show more
254 robust splicing changes than $1^{B/B};2^{A/A}$ mutants (Fig. 4). Consistent with the idea that
255 some exons were more sensitive to overall *mbnl* levels than others, some of the
256 alternative exons responded to loss of *mbnl1* function alone (*ank3b* exon 36, *atp2a1l*
257 exon 24, and *ryr1b* exon 72, Fig. 4A,B,C), while others required loss of both *mbnl1* and
258 *mbnl2* function for a splicing change to occur (*tpd52l2b* exon 4 and *csnk1da* exon 9, Fig.
259 4D,E).

260 **Mutation of *mbnl* genes led to decreased zebrafish size**

261 Mouse compound *Mbnl* loss of function mutants, but not single mutants, were
262 significantly smaller than WT mice (Lee et al., 2013; Thomas et al., 2017). To determine
263 whether loss of *mbnl* function had a similar effect in zebrafish, we raised WT, double
264 homozygous *mbnl* mutant, and triple homozygous *mbnl* mutant fish together in the
265 same tank and measured their lengths in early adulthood. WT fish were significantly
266 larger than $1^{B/B};3^{C/C}$ fish, which in turn were significantly larger than $1^{B/B};2^{A/A}$ fish (Fig.
267 5A). $2^{A/A};3^{C/C}$ fish were slightly smaller than WT fish, but the difference was not
268 statistically significant (Fig. 5A). Triple homozygous *mbnl* mutant fish were similar in
269 size to $1^{B/B};2^{A/A}$ fish (Fig. 5A). Interestingly, mutation of *mbnl1*, *mbnl2,* or *mbnl3* alone
270 was not sufficient to decrease adult zebrafish size (Fig. S4A,B,C). Taken together,
271 these results suggested that loss of function of more than one Mbnl protein was
272 required to reduce fish size, and that *mbnl1* had the strongest effect on fish size, *mbnl2*
273 played a smaller role, and *mbnl3* contributed minimally to adult fish size.

274 To assess whether zebrafish *mbnl* mutants had a developmental size phenotype,
275 we measured 7 dpf larval fish whose nutrition was derived from the yolk rather than
276 feeding. All double homozygous *mbnl* mutant larvae were similar in size to WT, except
277 for $2^{A/A};3^{C/C}$ larvae, which were slightly smaller than WT (Fig. 5B). $1^{B/B};2^{A/A};3^{C/C}$ larvae
278 were similar in size to their $1^{+/B};2^{A/A};3^{C/C}$ and $2^{A/A};3^{C/C}$ clutch mates, and all single
279 homozygous *mbnl* mutant larvae were either similar in size or slightly larger than WT
280 (Figs 5C and S4D). These results suggest that the reduced size phenotype in zebrafish
281 *mbnl* mutants arose later in development, after feeding began.

282 Histological analysis of adult skeletal muscle was performed by an expert
283 zebrafish pathologist to determine whether the fish genotypes with the most profound
284 size and splicing phenotypes, $1^{B/B;}2^{A/A}$ and $1^{B/B};2^{A/A};3^{C/C}$, also had changes in adult
285 muscle fiber morphology. We did not observe obvious signs of DM-related muscle
286 histopathology in the *mbnl* mutant fish (Fig S5), such as myofiber atrophy or centralized
287 nuclei as has been described in compound *mbnl* mutant mice and in individuals with DM
288 (Thomas et al., 2018; Thomas et al., 2017), but we cannot rule out the possibility that
289 the mutant fish had subtle alterations in muscle structure or function.

290 **Zebrafish *mbnl* mutants had altered movement**

291 Given that individuals with DM have impaired motor function, we asked whether
292 zebrafish *mbnl* mutants exhibited altered swimming behavior. We performed a test in
293 which individual adult fish were introduced to a novel tank and their position within the
294 tank was tracked for five minutes (Fig. 6A,B). A similar test was previously performed in
295 DM patients, in which the distance walked in six minutes was used as a measure of
296 motor function (Kierkegaard and Tollback, 2007; Park et al., 2018). While all single
297 homozygous mutants swam equal or greater distance than WT, two of the double
298 homozygous *mbnl* mutants ($1^{B/B};2^{A/A}$ and $1^{B/B};3^{C/C}$) and the $1^{B/B};2^{A/A};3^{C/C}$ mutants swam
299 significantly decreased distances compared to WT (Fig. 6C). One explanation for this
300 result is impaired motor function, although this phenotype needs to be explored further.
301 While performing these tests, we noticed a striking difference in the amount of time
302 *mbnl* mutants and WT fish spent near the bottom of the tank. We quantified this by
303 measuring the distance from the bottom of the tank in each frame for each fish and
304 averaging this over the recording period. Except for $2^{A/A};3^{C/C}$ mutants, all *mbnl* mutants
305 spent significantly more time toward the bottom of the tank than WT fish (Fig. 6D).
306 Avoiding the top of the tank is a well-known indicator of anxiety in zebrafish, and future
307 tests will explore whether *mbnl* mutants exhibit other signs of anxiety or perhaps have a
308 morphological or motor deficit that explains their lower swimming position (Cachat et al.,
309 2010). Overall, these results indicated that loss of *mbnl* function resulted in altered
310 movement in fish, but the exact mechanisms underlying these changes are unknown.
311

312 **Discussion**

313 For the first time, we generated a complete panel of vertebrate *mbnl* single,
314 double, and triple homozygous loss of function mutants. These mutants will be
315 invaluable for investigating the functions of vertebrate Mbnl proteins both individually
316 and in concert on an organismal level. Existing *Mbnl* mutant mice have provided
317 important insights into the biological functions of individual Mbnl proteins (Charizanis et
318 al., 2012; Choi et al., 2016; Kanadia et al., 2003; Lee et al., 2013; Poulos et al., 2013;
319 Thomas et al., 2017). However, the compound *Mbnl* mutant mouse models that most
320 closely mimic DM phenotypes are challenging to breed in large numbers and most die
321 during the neonatal period, making studies of adult phenotypes difficult. In contrast, all
322 double and triple homozygous *mbnl* mutant zebrafish are viable to adulthood, and fertile
323 double homozygous mutants can be incrossed to generate hundreds of mutants for
324 experiments. Even triple homozygous *mbnl* mutants, which do not mate on their own,
325 can be generated in large numbers through *in vitro* fertilization or through incrosses of
326 $1^{+/B};2^{A/A};3^{C/C}$ fish. The ability to study hundreds of zebrafish mutants at once provides
327 the statistical power to analyze subtle or variable phenotypes.

328 We propose a few explanations for why zebrafish $1^{B/B};2^{A/A}$ and $1^{B/B};2^{A/A};3^{C/C}$
329 mutants were viable to adulthood. Most muscle-specific double and triple *Mbnl* mutant
330 mice died during the neonatal period when they transitioned abruptly between receiving
331 oxygen through the placenta and breathing on their own. The small fraction of muscle-
332 specific compound *Mbnl* mutant mice that were able to make it through this transition
333 survived to adulthood (Thomas et al., 2018). In contrast, larval fish underwent a much
334 more gradual transition between receiving oxygen through diffusion to receiving oxygen
335 through the gills, and thus may have been better able to overcome this developmental
336 hurdle. Another possibility is that one or more of the zebrafish *mbnl* CRISPR mutations
337 did not result in a complete loss of function. In particular, $2^{A/A}$ mutants had the potential
338 to produce a partially functional protein containing one of the two sets of zinc finger
339 motifs (Fig. 1B), although we are confident that $2^{A/A}$ mutants represented at least a
340 partial loss of function given their splicing phenotypes and reduced *mbnl2* mRNA levels
341 (Figs 2,3,S1). Larvae injected with *mbnl2* morpholinos were reported to have dramatic

342 morphological phenotypes (Machuca-Tzili et al., 2011), although we were unable to
343 recapitulate these results (data not shown). The fact that our *2*$^{A/A}$ fish did not exhibit
344 similar phenotypes could be explained by partially retained Mbnl2 function in *2*$^{A/A}$ fish.
345 We suspect, however, that off target effects of the *Mbnl2* morpholinos contributed to the
346 observed morphological defects, given the mild phenotypes of *Mbnl2*$^{-/-}$ mice(Charizanis
347 et al., 2012).

348 Zebrafish *mbnl* mutants exhibited many of the same alternative splicing changes
349 that were observed in DM, FECD, and mouse DM models, suggesting that the splicing
350 targets of Mbnl proteins were conserved across species (Figs 2,3,4) (Bachinski et al.,
351 2014; Freyermuth et al., 2016; Goodwin et al., 2015; Hino et al., 2007; Kimura et al.,
352 2005). Similar to previous findings in mice, *mbnl1* and *mbnl2* played a larger role in
353 zebrafish splicing regulation than *mbnl3* for the exons tested (Figs 2,3,4) (Choi et al.,
354 2016; Poulos et al., 2013). Also consistent with mouse studies was the finding that
355 splicing changes tended to be larger in double homozygous zebrafish mutants than in
356 single homozygous mutants, suggesting partially overlapping functions of mbnl proteins
357 (Figs 2,3,4) (Lee et al., 2013; Thomas et al., 2017). Splicing changes in zebrafish *mbnl*
358 mutants occured in both larvae and adults, and across many DM-relevant tissues
359 (skeletal muscle, heart, brain, and intestine) as well as in the cornea, the tissue affected
360 in FECD.

361 Our data indicated that, just like other model organisms, zebrafish Mbnl-mediated
362 alternative splicing regulation was quite complex. Mbnl proteins suppressed inclusion of
363 some exons (*mbnl1* exon 5, *mbnl2* exon 5, *ank3b* exon 36, *tpd52l2b* exon 4, and
364 *csnk1da* exon 9), while they promoted inclusion of others (*ryr1b* exon 72 and *atp2a1l*
365 exon 24) (Figs 2,4). Similar to observations in other systems, some zebrafish exons
366 were more sensitive to changes in overall *mbnl* concentration than others (Wagner et
367 al., 2016). For example, in skeletal muscle, *mbnl2* exon 5 required the loss of both
368 *mbnl1* and *mbnl2* function for increased inclusion, whereas *mbnl1* exon 5 only required
369 the loss of *mbnl1* function (Fig. 2C,D).

370 An immediate future goal of ours is to perform a genome wide analysis of RNA
371 processing and expression changes in our complete panel of zebrafish *mbnl* mutants.

372 This will allow us to gain an understanding of how each Mbnl protein contributes to RNA
373 processing on a global level. It will identify candidate RNA processing events to
374 investigate further for relevance to disease phenotypes. A global analysis will also
375 enable us to determine the extent to which changes in RNA processing overlap
376 between zebrafish *mbnl* mutants and human patients with *MBNL* loss of function
377 disorders. While we demonstrated that the misregulation of several disease-relevant
378 alternative exons was conserved between human DM and FECD patients and zebrafish
379 models, not all missplicing events were conserved between species. For example,
380 zebrafish do not appear to have an ortholog of the *CLCN1* exon whose misregulation
381 contributed to myotonia in DM, so the zebrafish is unlikely to be an appropriate model
382 for studying myotonia, although it can be used to study many other important disease
383 phenotypes (Lueck et al., 2007a; Lueck et al., 2007b).
384 In addition to their molecular phenotypes, zebrafish *mbnl* mutants had physical
385 phenotypes that were relevant to human disease and mouse models. Adult $1^{B/B};2^{A/A}$,
386 $1^{B/B};3^{C/C}$, and $1^{B/B};2^{A/A};3^{C/C}$ fish were significantly smaller than their WT tank mates (Fig.
387 5A). Neonatal muscle-specific compound mutant mice likewise were substantially
388 smaller than their littermates (Thomas et al., 2017). In the case of fish, the size
389 phenotype did not arise in early in development, as 7 dpf larval *mbnl* mutant fish were
390 not smaller than WT fish (Figs 5B,C and S4D). We do not know the mechanism
391 underlying the size phenotype in *mbnl* mutant fish, but one possibility is impaired
392 swimming ability, leading to decreased ability to compete with tank mates for access to
393 food. Consistent with this idea, we found that $1^{B/B};2^{A/A}$, $1^{B/B};3^{C/C}$, and $1^{B/B};2^{A/A};3^{C/C}$ fish
394 swam a significantly decreased distance compared to WT fish during a five-minute swim
395 test (Fig. 6B,C). Interestingly, human DM patients exhibited decreased performance on
396 a similar 6-minute walk test due to muscle weakness and impaired motor function,
397 leading us to hypothesize that *mbnl* mutant fish also had muscle weakness
398 (Kierkegaard and Tollback, 2007; Park et al., 2018). Although basic histological
399 analysis did not indicate obvious signs of muscle fiber pathology in *mbnl* mutant fish
400 (Fig. S5), more in-depth analyses are needed to determine whether subtle changes in
401 muscle structure or function are present that could lead to muscle weakness. We also

402 found that all genotypes of *mbnl* mutant fish stayed closer to the bottom of the tank on
403 average than WT fish (Fig. 6B,D), which could also decrease access to food as fish
404 were fed from the top of the tank. The *mbnl* mutant fish could have stayed at the
405 bottom of the tank due to motor dysfunction or a morphological defect, but this
406 phenotype is also a well-characterized indicator of anxiety in fish (Cachat et al., 2010).
407 Individuals with DM often show signs of avoidant personality disorder with anxiety, and
408 an intriguing possibility is that *mbnl* mutant fish also have increased anxiety (Delaporte,
409 1998; Minier et al., 2018). Our future studies will explore in depth the mechanisms
410 underlying decreased size and altered swimming behavior in *mbnl* mutant fish.
411 In summary, we successfully generated a complete panel of zebrafish single,
412 double, and triple homozygous *mbnl* mutants for modeling human *mbnl* loss of function
413 disorders. These fish exhibited molecular and physical phenotypes similar to those
414 observed in humans with FECD and DM. The new models will be highly useful in future
415 studies of the functions of individual Mbnl proteins and how they contribute to disease
416 relevant phenotypes. Strengths of using zebrafish over other vertebrate model systems
417 are that large numbers of fish can be generated to study subtle or variable phenotypes,
418 and the fact that transparent larvae can be used to directly study disease-related
419 phenotypes, such as altered gut motility and heart abnormalities, in live animals.

420 **Materials and Methods**

421 Generation of mutant zebrafish

422 All zebrafish experiments were performed with the guidance and approval of the
423 University of Oregon Institutional Animal Care and Use Committee. Guide RNAs
424 (gRNAs) targeting zebrafish (*Danio rerio*) *mbnl1*, *mbnl2*, and *mbnl3* were designed
425 using the Chop Chop website (http://chopchop.cbu.uib.no). DNA templates for the
426 gRNAs were generated by a template-free Phusion polymerase (New England Biolabs)
427 PCR reaction using a common scaffold primer (gRNA scaffold, Table S1) and a gene-
428 specific primer (*mbnl1* gRNA1, *mbnl1* gRNA2, *mbnl2* gRNA, *mbnl3* gRNA1, or *mbnl3*
429 gRNA2, Table S1), then cleaned using the QIAquick PCR Purification Kit (Qiagen).
430 gRNAs were transcribed from DNA templates using a MEGAscript kit (Ambion) and
431 purified by phenol-chloroform extraction and isopropanol precipitation. Cas9 RNA was

432 generated by linearizing the pT3TS-nls-zCas9-nls plasmid (Jao et al., 2013) with XbaI,
433 purifying it using the QIAquick Gel Extraction Kit (Qiagen), performing an in vitro
434 transcription reaction using the T3 mMESSAGE kit (Invitrogen), and purifying the RNA
435 using the RNeasy Mini kit (Qiagen). AB zebrafish embryos were microinjected at the
436 one cell stage with 1-2 nL of a mixture containing 100ng/μL Cas9 mRNA, 50 ng/μL
437 gRNA, and phenol red, and raised to adulthood. Mosaic mutants were identified by
438 PCR amplification and Sanger sequencing of fin clip DNA using primers specific to the
439 targeted region (Tables S1,S2), and outcrossed to wildtype AB zebrafish to generate
440 heterozygotes. Fish with predicted loss of function mutations were identified by Sanger
441 sequencing (Table S2), and further crossed to generate single, double, and triple *mbnl1*,
442 *mbnl2*, and *mbnl3* homozygotes. Fish were genotyped by restriction fragment length
443 polymorphism analysis using the primers and restriction enzymes indicated in Table S2.
444 Sperm from all zebrafish mutant lines were cryopreserved and are available upon
445 request from the corresponding author.

446 Measurement of zebrafish size

447 Young adult fish (2-4 months old) (Figs 5A,S4A,B,C) were anesthetized in 168
448 mg/L tricaine methane sulfonate, photographed against a white background with a ruler
449 using a tablet computer, finclipped, and genotyped. To ensure identical density and
450 feeding conditions, fish were compared with others from the same clutch (Fig. S4A,B,C)
451 or different clutches that had been raised together in the same tank (Fig. 5A). For
452 measurement of larval fish, unfed embryos of different genotypes were raised to 7 days
453 post fertilization (dpf) in separate dishes at a density of one fish per mL of embryo
454 medium, with the exception of the larvae in Fig. 5C, which were grown in the same dish
455 and genotyped after measurement. Fish were anesthetized in 168 mg/mL tricaine
456 methane sulfonate, laid out on a microscope slide in 3% methylcellulose, and imaged
457 using a Leica M165FC microscope. An investigator that was blinded to genotype
458 measured the distance from snout to caudal peduncle or posterior tip of the notochord
459 (standard length, SL) of each fish (Parichy et al., 2009). Data were analyzed by
460 ordinary one-way ANOVA with multiple comparison correction.

461 Alternative splicing analysis

462 Fish were euthanized by tricaine methane sulfonate overdose (larvae) or
463 hypothermic shock (adults). Tissues of interest were dissected and flash frozen in 1 mL
464 of Trizol (Ambion), thawed, and homogenized with a mortar and pestle (larvae) or Bullet
465 Blender Storm 24 (adult tissues). Chloroform (200 μL) was added to each tube followed
466 by mixing, centrifugation at 12,000 g for 10 minutes at 4°C, transfer of the aqueous
467 phase to a separate tube, addition of 200 μL ethanol, and binding of sample to an
468 RNeasy mini kit column (Qiagen). RNA was washed and eluted according to the
469 manufacturer's instructions and the concentration was measured using a NanoDrop
470 2000 (Thermo Scientific).
471 RNA (20-200 ng) was reverse transcribed with Superscript II Reverse
472 Transcriptase (Invitrogen) according to the manufacturer's instructions using gene-
473 specific reverse (R) primers located in the exon downstream of the regulated exon of
474 interest (Table S1). The resulting cDNA was amplified by 28-31 cycles of PCR using
475 Taq polymerase and the forward (F) and reverse (R) primers indicated in Table S1.
476 Samples were separated by electrophoresis on a 6% *bis*-Acrylamide (19:1) gel that was
477 stained overnight with 1X SYBR green I nucleic acid gel stain (Invitrogen). The gel was
478 imaged and quantified using an AlphaImagerHP (Alpha Innotech). The background-
479 corrected sum of each band was measured and the percent exon inclusion was
480 calculated using the following formula: ((exon included sum) /(exon included sum +
481 exon excluded sum)) X 100. Data were analyzed by ordinary one-way ANOVA with
482 multiple comparison correction.
483 <u>RT-qPCR</u>
484 Total RNA was prepared from 5 dpf larvae and adult tissues using the same
485 procedure as for alternative splicing analysis. RNA was treated with TURBO DNase
486 (Ambion) according to manufacturer's instructions then reverse transcribed with an
487 oligo$(dT)_{20}$ primer using the Superscript III cDNA First Strand Synthesis kit (Invitrogen).
488 The qPCR reaction was set up using the KAPA SYBR FAST ABI Prism kit (KAPA
489 Biosystems) according to manufacturer's instructions and run on a Quant Studio 3
490 System (ThermoFisher) using the default settings for SYBR Green reagents and the
491 fast run mode in the QuantStudio Design & Analysis Software v.1.4.2. The comparative

492 C_T ($\Delta\Delta C_T$) method was used to calculate relative mRNA levels. Five biological samples
493 of each genotype or tissue type were run in triplicate and data were normalized to the
494 expression of the housekeeping gene *eef1a1l1*(Vanhauwaert et al., 2014). Primers
495 used for RT-qPCR are shown in Table S1.

496 Zebrafish behavior assays

497 Age-matched single adult zebrafish were placed into a novel environment
498 consisting of a custom glass aquarium measuring 18 cm deep X 25.4 cm long X 7.6 cm
499 wide (Fig. 6A). The fish were monitored with a Logitech camera during a 5 minute time
500 frame to characterize basic exploratory swimming behavior. The raw tracking data was
501 analyzed with custom software (DaniOPEN, https://github.com/stednitzs/daniopen) to
502 measure swim distance and distance from the bottom of the tank(Stednitz et al., 2018).
503 Following the test period, the fish were returned to their home tanks.

504 Histology

505 Ten-month-old WT and mutant adult zebrafish were euthanized by hypothermic
506 shock and fixed in Bouin's solution (Sigma), then washed in 70% ethanol. Fixed fish
507 were bisected parasagitally or transversely, processed for paraffin embedding,
508 sectioned at 7 μm thickness, and stained with hematoxylin and eosin by a histologist
509 from the University of Oregon Institute of Neuroscience. Muscle morphology was
510 analyzed by a zebrafish pathologist from the Zebrafish International Resource Center
511 who was blinded to genotype. Representative DIC images of muscle transverse
512 sections were taken using a Leica DMLB microscope.

513 **Acknowledgements**

514 We thank the staff of the University of Oregon Zebrafish Facility for maintaining fish and
515 providing expertise in performing zebrafish procedures, and Dr. Poh Kheng Loi for
516 histological services. We thank Ellie Melancon, Camila Morales Fenero, Michelle
517 Massaquoi, and Sam Peterson for advice in performing experiments and data analysis,
518 and members of the Guillemin, Berglund, and Eisen labs for helpful discussions.

519 **Competing Interests**

520 No competing interests declared.

521

522 **Funding**

523 Research reported in this publication was supported by the National Institute of General
524 Medical Sciences of the National Institutes of Health under award numbers
525 1P50GM098911 and 1P01GM125576 to K.G. and 5R01GM121862 to J.A.B., and by
526 the National Institute of Diabetes and Digestive and Kidney Diseases of the National
527 Institutes of Health under award number F32DK107318 to M.N.H. It was also
528 supported by grants from the Muscular Dystrophy Association (516314 to J.A.B.) and
529 the Myotonic Dystrophy/Wyck Foundation (Wyck-FF-2014-0013 to M.N.H.). The
530 content is solely the responsibility of the authors and does not necessarily represent the
531 official views of the National Institutes of Health, the Muscular Dystrophy Association, or
532 the Myotonic Dystrophy/Wyck Foundation.

533

534 **References**

535 **Ashwal-Fluss, R., Meyer, M., Pamudurti, N. R., Ivanov, A., Bartok, O., Hanan,**
536 **M., Evantal, N., Memczak, S., Rajewsky, N. and Kadener, S.** (2014). circRNA
537 biogenesis competes with pre-mRNA splicing. *Mol Cell* **56**, 55-66.
538 **Bachinski, L. L., Baggerly, K. A., Neubauer, V. L., Nixon, T. J., Raheem, O.,**
539 **Sirito, M., Unruh, A. K., Zhang, J., Nagarajan, L., Timchenko, L. T. et al.** (2014).
540 Most expression and splicing changes in myotonic dystrophy type 1 and type 2 skeletal
541 muscle are shared with other muscular dystrophies. *Neuromuscul Disord* **24**, 227-40.
542 **Batra, R., Charizanis, K., Manchanda, M., Mohan, A., Li, M., Finn, D. J.,**
543 **Goodwin, M., Zhang, C., Sobczak, K., Thornton, C. A. et al.** (2014). Loss of MBNL
544 leads to disruption of developmentally regulated alternative polyadenylation in RNA-
545 mediated disease. *Mol Cell* **56**, 311-322.
546 **Bellini, M., Biagi, S., Stasi, C., Costa, F., Mumolo, M. G., Ricchiuti, A. and**
547 **Marchi, S.** (2006). Gastrointestinal manifestations in myotonic muscular dystrophy.
548 *World J Gastroenterol* **12**, 1821-8.
549 **Brook, J. D., McCurrach, M. E., Harley, H. G., Buckler, A. J., Church, D.,**
550 **Aburatani, H., Hunter, K., Stanton, V. P., Thirion, J. P., Hudson, T. et al.** (1992).
551 Molecular basis of myotonic dystrophy: expansion of a trinucleotide (CTG) repeat at the
552 3' end of a transcript encoding a protein kinase family member. *Cell* **68**, 799-808.
553 **Cachat, J., Stewart, A., Grossman, L., Gaikwad, S., Kadri, F., Chung, K. M.,**
554 **Wu, N., Wong, K., Roy, S., Suciu, C. et al.** (2010). Measuring behavioral and
555 endocrine responses to novelty stress in adult zebrafish. *Nat Protoc* **5**, 1786-99.
556 **Charizanis, K., Lee, K. Y., Batra, R., Goodwin, M., Zhang, C., Yuan, Y.,**
557 **Shiue, L., Cline, M., Scotti, M. M., Xia, G. et al.** (2012). Muscleblind-like 2-mediated
558 alternative splicing in the developing brain and dysregulation in myotonic dystrophy.
559 *Neuron* **75**, 437-50.
560 **Choi, J., Dixon, D. M., Dansithong, W., Abdallah, W. F., Roos, K. P., Jordan,**
561 **M. C., Trac, B., Lee, H. S., Comai, L. and Reddy, S.** (2016). Muscleblind-like 3 deficit
562 results in a spectrum of age-associated pathologies observed in myotonic dystrophy.
563 *Sci Rep* **6**, 30999.
564 **Delaporte, C.** (1998). Personality patterns in patients with myotonic dystrophy.
565 *Arch Neurol* **55**, 635-40.
566 **Du, H., Cline, M. S., Osborne, R. J., Tuttle, D. L., Clark, T. A., Donohue, J. P.,**
567 **Hall, M. P., Shiue, L., Swanson, M. S., Thornton, C. A. et al.** (2010). Aberrant
568 alternative splicing and extracellular matrix gene expression in mouse models of
569 myotonic dystrophy. *Nat Struct Mol Biol* **17**, 187-93.
570 **Du, J., Aleff, R. A., Soragni, E., Kalari, K., Nie, J., Tang, X., Davila, J.,**
571 **Kocher, J. P., Patel, S. V., Gottesfeld, J. M. et al.** (2015). RNA toxicity and missplicing
572 in the common eye disease fuchs endothelial corneal dystrophy. *J Biol Chem* **290**,
573 5979-90.
574 **Fardaei, M., Rogers, M. T., Thorpe, H. M., Larkin, K., Hamshere, M. G.,**
575 **Harper, P. S. and Brook, J. D.** (2002). Three proteins, MBNL, MBLL and MBXL, co-
576 localize in vivo with nuclear foci of expanded-repeat transcripts in DM1 and DM2 cells.
577 *Hum Mol Genet* **11**, 805-14.

578 **Freyermuth, F., Rau, F., Kokunai, Y., Linke, T., Sellier, C., Nakamori, M.,**
579 **Kino, Y., Arandel, L., Jollet, A., Thibault, C. et al.** (2016). Splicing misregulation of
580 SCN5A contributes to cardiac-conduction delay and heart arrhythmia in myotonic
581 dystrophy. *Nat Commun* **7**, 11067.
582 **Fu, Y. H., Pizzuti, A., Fenwick, R. G., Jr., King, J., Rajnarayan, S., Dunne, P.**
583 **W., Dubel, J., Nasser, G. A., Ashizawa, T., de Jong, P. et al.** (1992). An unstable
584 triplet repeat in a gene related to myotonic muscular dystrophy. *Science* **255**, 1256-8.
585 **Gates, D. P., Coonrod, L. A. and Berglund, J. A.** (2011). Autoregulated splicing
586 of muscleblind-like 1 (MBNL1) Pre-mRNA. *J Biol Chem* **286**, 34224-33.
587 **Goers, E. S., Purcell, J., Voelker, R. B., Gates, D. P. and Berglund, J. A.**
588 (2010). MBNL1 binds GC motifs embedded in pyrimidines to regulate alternative
589 splicing. *Nucleic Acids Res* **38**, 2467-84.
590 **Goodwin, M., Mohan, A., Batra, R., Lee, K. Y., Charizanis, K., Fernandez**
591 **Gomez, F. J., Eddarkaoui, S., Sergeant, N., Buee, L., Kimura, T. et al.** (2015). MBNL
592 Sequestration by Toxic RNAs and RNA Misprocessing in the Myotonic Dystrophy Brain.
593 *Cell Rep* **12**, 1159-68.
594 **Grammatikakis, I., Goo, Y. H., Echeverria, G. V. and Cooper, T. A.** (2011).
595 Identification of MBNL1 and MBNL3 domains required for splicing activation and
596 repression. *Nucleic Acids Res* **39**, 2769-80.
597 **Hilbert, J. E., Barohn, R. J., Clemens, P. R., Luebbe, E. A., Martens, W. B.,**
598 **McDermott, M. P., Parkhill, A. L., Tawil, R., Thornton, C. A., Moxley, R. T., 3rd et al.**
599 (2017). High frequency of gastrointestinal manifestations in myotonic dystrophy type 1
600 and type 2. *Neurology* **89**, 1348-1354.
601 **Hino, S., Kondo, S., Sekiya, H., Saito, A., Kanemoto, S., Murakami, T.,**
602 **Chihara, K., Aoki, Y., Nakamori, M., Takahashi, M. P. et al.** (2007). Molecular
603 mechanisms responsible for aberrant splicing of SERCA1 in myotonic dystrophy type 1.
604 *Hum Mol Genet* **16**, 2834-43.
605 **Ho, T. H., Charlet, B. N., Poulos, M. G., Singh, G., Swanson, M. S. and**
606 **Cooper, T. A.** (2004). Muscleblind proteins regulate alternative splicing. *EMBO J* **23**,
607 3103-12.
608 **Jao, L. E., Wente, S. R. and Chen, W.** (2013). Efficient multiplex biallelic
609 zebrafish genome editing using a CRISPR nuclease system. *Proc Natl Acad Sci U S A*
610 **110**, 13904-9.
611 **Kalsotra, A., Xiao, X., Ward, A. J., Castle, J. C., Johnson, J. M., Burge, C. B.**
612 **and Cooper, T. A.** (2008). A postnatal switch of CELF and MBNL proteins reprograms
613 alternative splicing in the developing heart. *Proc Natl Acad Sci U S A* **105**, 20333-8.
614 **Kanadia, R. N., Johnstone, K. A., Mankodi, A., Lungu, C., Thornton, C. A.,**
615 **Esson, D., Timmers, A. M., Hauswirth, W. W. and Swanson, M. S.** (2003). A
616 muscleblind knockout model for myotonic dystrophy. *Science* **302**, 1978-80.
617 **Kierkegaard, M. and Tollback, A.** (2007). Reliability and feasibility of the six
618 minute walk test in subjects with myotonic dystrophy. *Neuromuscul Disord* **17**, 943-9.
619 **Kimura, T., Nakamori, M., Lueck, J. D., Pouliquin, P., Aoike, F., Fujimura, H.,**
620 **Dirksen, R. T., Takahashi, M. P., Dulhunty, A. F. and Sakoda, S.** (2005). Altered
621 mRNA splicing of the skeletal muscle ryanodine receptor and

622 sarcoplasmic/endoplasmic reticulum Ca2+-ATPase in myotonic dystrophy type 1. *Hum*
623 *Mol Genet* **14**, 2189-200.
624 **Lee, K. Y., Li, M., Manchanda, M., Batra, R., Charizanis, K., Mohan, A.,**
625 **Warren, S. A., Chamberlain, C. M., Finn, D., Hong, H. et al.** (2013). Compound loss
626 of muscleblind-like function in myotonic dystrophy. *EMBO Mol Med* **5**, 1887-900.
627 **Lin, X., Miller, J. W., Mankodi, A., Kanadia, R. N., Yuan, Y., Moxley, R. T.,**
628 **Swanson, M. S. and Thornton, C. A.** (2006). Failure of MBNL1-dependent post-natal
629 splicing transitions in myotonic dystrophy. *Hum Mol Genet* **15**, 2087-97.
630 **Liquori, C. L., Ricker, K., Moseley, M. L., Jacobsen, J. F., Kress, W., Naylor,**
631 **S. L., Day, J. W. and Ranum, L. P.** (2001). Myotonic dystrophy type 2 caused by a
632 CCTG expansion in intron 1 of ZNF9. *Science* **293**, 864-7.
633 **Liu, Y. F., Liu, H. Y., Tu, L. C., Lin, C. W., Hsiao, K. M. and Pan, H.** (2008).
634 Zebrafish muscleblind-like genes: identification, structural features and expression.
635 *Comp Biochem Physiol B Biochem Mol Biol* **151**, 118-24.
636 **Lueck, J. D., Lungu, C., Mankodi, A., Osborne, R. J., Welle, S. L., Dirksen, R.**
637 **T. and Thornton, C. A.** (2007a). Chloride channelopathy in myotonic dystrophy
638 resulting from loss of posttranscriptional regulation for CLCN1. *Am J Physiol Cell*
639 *Physiol* **292**, C1291-7.
640 **Lueck, J. D., Mankodi, A., Swanson, M. S., Thornton, C. A. and Dirksen, R.**
641 **T.** (2007b). Muscle chloride channel dysfunction in two mouse models of myotonic
642 dystrophy. *J Gen Physiol* **129**, 79-94.
643 **Machuca-Tzili, L. E., Buxton, S., Thorpe, A., Timson, C. M., Wigmore, P.,**
644 **Luther, P. K. and Brook, J. D.** (2011). Zebrafish deficient for Muscleblind-like 2 exhibit
645 features of myotonic dystrophy. *Dis Model Mech* **4**, 381-92.
646 **Mahadevan, M., Tsilfidis, C., Sabourin, L., Shutler, G., Amemiya, C., Jansen,**
647 **G., Neville, C., Narang, M., Barcelo, J., O'Hoy, K. et al.** (1992). Myotonic dystrophy
648 mutation: an unstable CTG repeat in the 3' untranslated region of the gene. *Science*
649 **255**, 1253-5.
650 **Miller, J. W., Urbinati, C. R., Teng-Umnuay, P., Stenberg, M. G., Byrne, B. J.,**
651 **Thornton, C. A. and Swanson, M. S.** (2000). Recruitment of human muscleblind
652 proteins to (CUG)(n) expansions associated with myotonic dystrophy. *EMBO J* **19**,
653 4439-48.
654 **Minier, L., Lignier, B., Bouvet, C., Gallais, B. and Camart, N.** (2018). A
655 Review of Psychopathology Features, Personality, and Coping in Myotonic Dystrophy
656 Type 1. *J Neuromuscul Dis* **5**, 279-294.
657 **Mootha, V. V., Hansen, B., Rong, Z., Mammen, P. P., Zhou, Z., Xing, C. and**
658 **Gong, X.** (2017). Fuchs' Endothelial Corneal Dystrophy and RNA Foci in Patients With
659 Myotonic Dystrophy. *Invest Ophthalmol Vis Sci* **58**, 4579-4585.
660 **Mootha, V. V., Hussain, I., Cunnusamy, K., Graham, E., Gong, X., Neelam,**
661 **S., Xing, C., Kittler, R. and Petroll, W. M.** (2015). TCF4 Triplet Repeat Expansion and
662 Nuclear RNA Foci in Fuchs' Endothelial Corneal Dystrophy. *Invest Ophthalmol Vis Sci*
663 **56**, 2003-11.

Oddo, J. C., Saxena, T., McConnell, O. L., Berglund, J. A. and Wang, E. T. (2016). Conservation of context-dependent splicing activity in distant Muscleblind homologs. *Nucleic Acids Res* **44**, 8352-62.

Parichy, D. M., Elizondo, M. R., Mills, M. G., Gordon, T. N. and Engeszer, R. E. (2009). Normal table of postembryonic zebrafish development: staging by externally visible anatomy of the living fish. *Dev Dyn* **238**, 2975-3015.

Park, D., Lee, S. H., Shin, J. H. and Park, J. S. (2018). Lower limb muscle magnetic resonance imaging in myotonic dystrophy type 1 correlates with the six-minute walk test and CTG repeats. *Neuromuscul Disord* **28**, 29-37.

Poulos, M. G., Batra, R., Li, M., Yuan, Y., Zhang, C., Darnell, R. B. and Swanson, M. S. (2013). Progressive impairment of muscle regeneration in muscleblind-like 3 isoform knockout mice. *Hum Mol Genet* **22**, 3547-58.

Rau, F., Freyermuth, F., Fugier, C., Villemin, J. P., Fischer, M. C., Jost, B., Dembele, D., Gourdon, G., Nicole, A., Duboc, D. et al. (2011). Misregulation of miR-1 processing is associated with heart defects in myotonic dystrophy. *Nat Struct Mol Biol* **18**, 840-5.

Stednitz, S. J., McDermott, E. M., Ncube, D., Tallafuss, A., Eisen, J. S. and Washbourne, P. (2018). Forebrain Control of Behaviorally Driven Social Orienting in Zebrafish. *Curr Biol* **28**, 2445-2451 e3.

Tarnopolsky, M. A., Pearce, E., Matteliano, A., James, C. and Armstrong, D. (2010). Bacterial overgrowth syndrome in myotonic muscular dystrophy is potentially treatable. *Muscle Nerve* **42**, 853-5.

Terenzi, F. and Ladd, A. N. (2010). Conserved developmental alternative splicing of muscleblind-like (MBNL) transcripts regulates MBNL localization and activity. *RNA Biol* **7**, 43-55.

Thomas, J. D., Oliveira, R., Sznajder, L. J. and Swanson, M. S. (2018). Myotonic Dystrophy and Developmental Regulation of RNA Processing. *Compr Physiol* **8**, 509-553.

Thomas, J. D., Sznajder, L. J., Bardhi, O., Aslam, F. N., Anastasiadis, Z. P., Scotti, M. M., Nishino, I., Nakamori, M., Wang, E. T. and Swanson, M. S. (2017). Disrupted prenatal RNA processing and myogenesis in congenital myotonic dystrophy. *Genes Dev* **31**, 1122-1133.

Tieleman, A. A., van Vliet, J., Jansen, J. B., van der Kooi, A. J., Borm, G. F. and van Engelen, B. G. (2008). Gastrointestinal involvement is frequent in Myotonic Dystrophy type 2. *Neuromuscul Disord* **18**, 646-9.

Todd, P. K., Ackall, F. Y., Hur, J., Sharma, K., Paulson, H. L. and Dowling, J. J. (2014). Transcriptional changes and developmental abnormalities in a zebrafish model of myotonic dystrophy type 1. *Dis Model Mech* **7**, 143-55.

Tran, H., Gourrier, N., Lemercier-Neuillet, C., Dhaenens, C. M., Vautrin, A., Fernandez-Gomez, F. J., Arandel, L., Carpentier, C., Obriot, H., Eddarkaoui, S. et al. (2011). Analysis of exonic regions involved in nuclear localization, splicing activity, and dimerization of Muscleblind-like-1 isoforms. *J Biol Chem* **286**, 16435-46.

Vanhauwaert, S., Van Peer, G., Rihani, A., Janssens, E., Rondou, P., Lefever, S., De Paepe, A., Coucke, P. J., Speleman, F., Vandesompele, J. et al.

(2014). Expressed repeat elements improve RT-qPCR normalization across a wide range of zebrafish gene expression studies. *PLoS One* **9**, e109091.

Wagner, S. D., Struck, A. J., Gupta, R., Farnsworth, D. R., Mahady, A. E., Eichinger, K., Thornton, C. A., Wang, E. T. and Berglund, J. A. (2016). Dose-Dependent Regulation of Alternative Splicing by MBNL Proteins Reveals Biomarkers for Myotonic Dystrophy. *PLoS Genet* **12**, e1006316.

Wang, E. T., Cody, N. A., Jog, S., Biancolella, M., Wang, T. T., Treacy, D. J., Luo, S., Schroth, G. P., Housman, D. E., Reddy, S. et al. (2012). Transcriptome-wide regulation of pre-mRNA splicing and mRNA localization by muscleblind proteins. *Cell* **150**, 710-24.

Warf, M. B. and Berglund, J. A. (2007). MBNL binds similar RNA structures in the CUG repeats of myotonic dystrophy and its pre-mRNA substrate cardiac troponin T. *RNA* **13**, 2238-51.

Wenninger, S., Montagnese, F. and Schoser, B. (2018). Core Clinical Phenotypes in Myotonic Dystrophies. *Front Neurol* **9**, 303.

Wieben, E. D., Aleff, R. A., Tang, X., Butz, M. L., Kalari, K. R., Highsmith, E. W., Jen, J., Vasmatzis, G., Patel, S. V., Maguire, L. J. et al. (2017). Trinucleotide Repeat Expansion in the Transcription Factor 4 (TCF4) Gene Leads to Widespread mRNA Splicing Changes in Fuchs' Endothelial Corneal Dystrophy. *Invest Ophthalmol Vis Sci* **58**, 343-352.

Winkler, N. S., Milone, M., Martinez-Thompson, J. M., Raja, H., Aleff, R. A., Patel, S. V., Fautsch, M. P., Wieben, E. D. and Baratz, K. H. (2018). Fuchs' Endothelial Corneal Dystrophy in Patients With Myotonic Dystrophy, Type 1. *Invest Ophthalmol Vis Sci* **59**, 3053-3057.

Zhao, Y., Ogawa, H., Yonekura, S., Mitsuhashi, H., Mitsuhashi, S., Nishino, I., Toyoshima, C. and Ishiura, S. (2015). Functional analysis of SERCA1b, a highly expressed SERCA1 variant in myotonic dystrophy type 1 muscle. *Biochim Biophys Acta* **1852**, 2042-7.

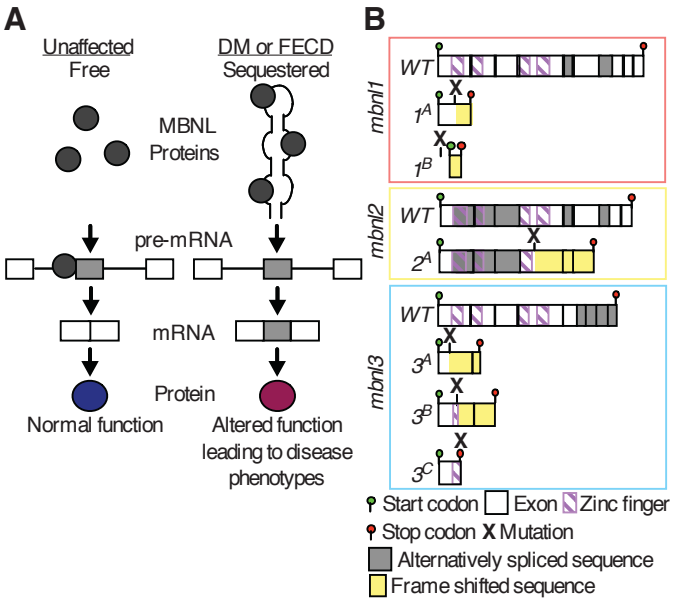

Figure 1 Zebrafish models of human *MBNL* loss of function disorders were generated by mutating *mbnl1, mbnl2,* and *mbnl3.* A. Primary molecular mechanism of the human MBNL loss of function disorders myotonic dystrophy (DM) and Fuchs endothelial corneal dystrophy (FECD). In unaffected individuals, free MBNL1, MBNL2, and MBNL3 proteins bind to target pre-mRNAs and regulate the inclusion of alternative exons in mRNAs. MBNL proteins suppress alternative exon inclusion in the example shown here, but they promote inclusion of other target alternative exons. In individuals with DM or FECD, MBNL proteins are sequestered by long CUG or CCUG repeat RNAs, which decreases their availability to bind to target pre-mRNAs and alters mRNA isoform production and downstream protein function. **B.** Diagram of WT and mutant zebrafish *mbnl1*, *mbnl2,* and *mbnl3* predicted coding sequences. Mutant sequences are shown in Table S2. *mbnl1* mutant alleles are denoted as 1^A and 1^B, *mbnl2* as 2^A, and *mbnl3* as $3^{A/A}$, $3^{B/B}$, and $3^{C/C}$.

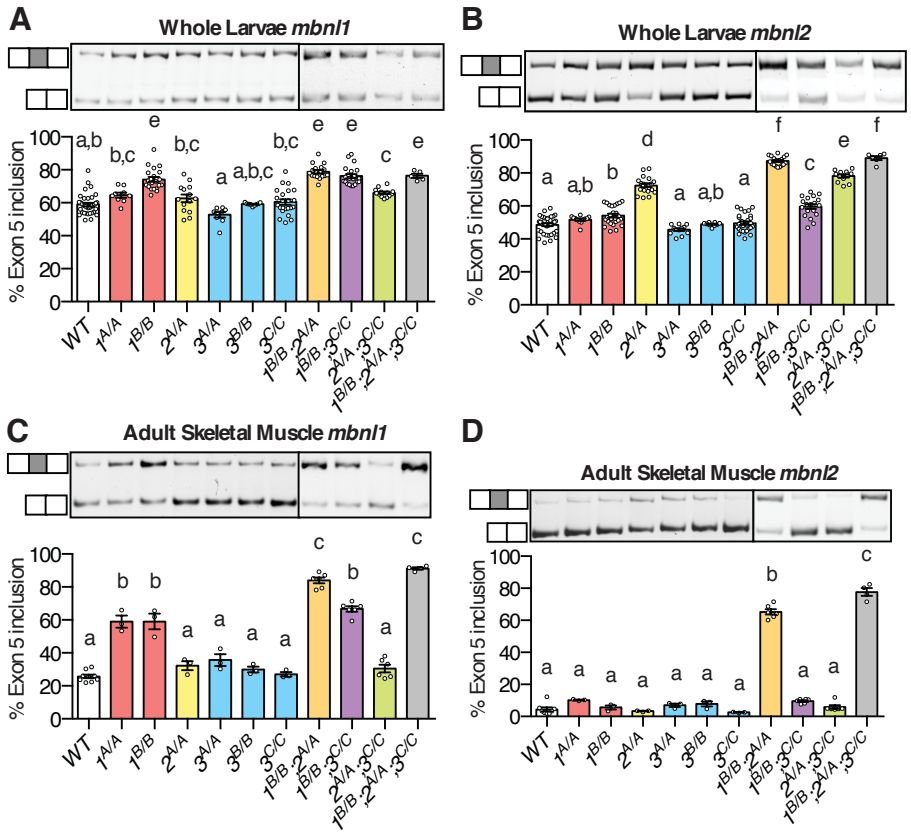

Figure 2 Misregulation of *mbnl* alternative splicing was conserved in zebrafish *mbnl* mutants. A & B. RT-PCR analysis showing inclusion of **(A)** *mbnl1* exon 5 or **(B)** *mbnl2* exon 5 in WT and *mbnl* mutant whole larval zebrafish at 5 days post fertilization (dpf). Each dot represents RNA pooled from 5 larvae. **C & D.** RT-PCR analysis showing inclusion of **(C)** *mbnl1* exon 5 or **(D)** *mbnl2* exon 5 in WT and *mbnl* mutant adult zebrafish skeletal muscle. Each dot represents RNA from one fish. Error bars indicate standard error of the mean. For all graphs, *mbnl1* mutant alleles are denoted as 1^A and 1^B, *mbnl2* alleles as 2^A, and *mbnl3* alleles as 3^A, 3^B, and 3^C. Representative RT-PCR gels are shown above each graph. Dividing lines indicated samples run on separate gels. Data were analyzed by ordinary one-way ANOVA with Tukey's multiple comparisons test. Data bars that do not share a letter above them are significantly different from one another.

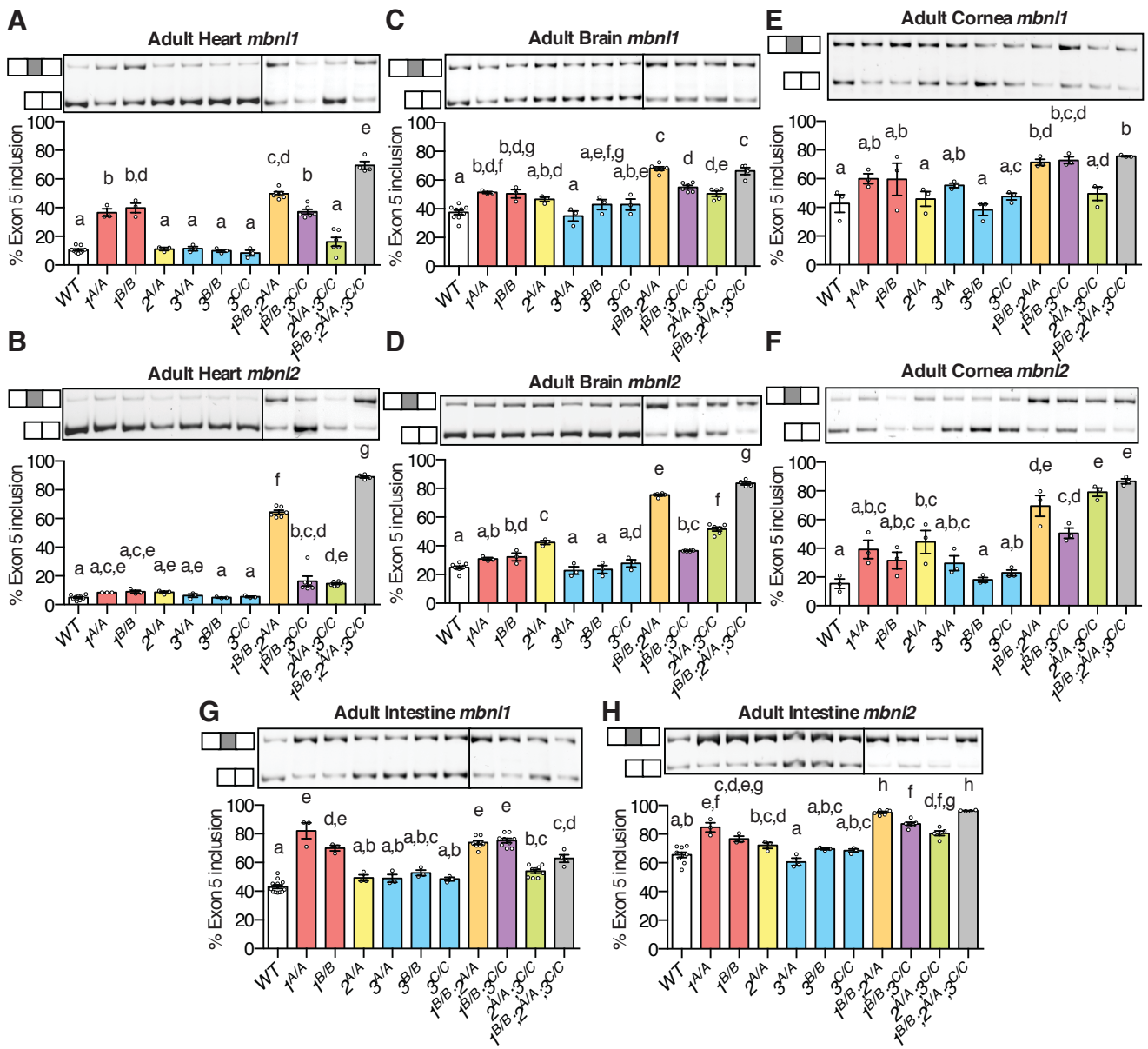

Figure 3 Alternative splicing of *mbnl1* and *mbnl2* was misregulated across tissues in zebrafish *mbnl* mutants. A-H. RT-PCR analysis showing inclusion of *mbnl1* exon 5 **(A, C, E, & G)** or *mbnl2* exon 5 **(B, D, F, & H)** in WT and *mbnl* mutant adult zebrafish heart **(A & B)**, brain **(C & D)**, cornea **(E &F)**, and intestine **(G & H)**. For all graphs, *mbnl1* mutant alleles are denoted as 1^A and 1^B, *mbnl2* alleles as 2^A, and *mbnl3* alleles as 3^A, 3^B, and 3^C. Each dot represents RNA from one fish. Error bars indicate standard error of the mean. Representative RT-PCR gels are shown above each graph. Dividing lines indicated samples run on separate gels. Data were analyzed by ordinary one-way ANOVA with Tukey's multiple comparisons test. Data bars that do not share a letter above them are significantly different from one another.

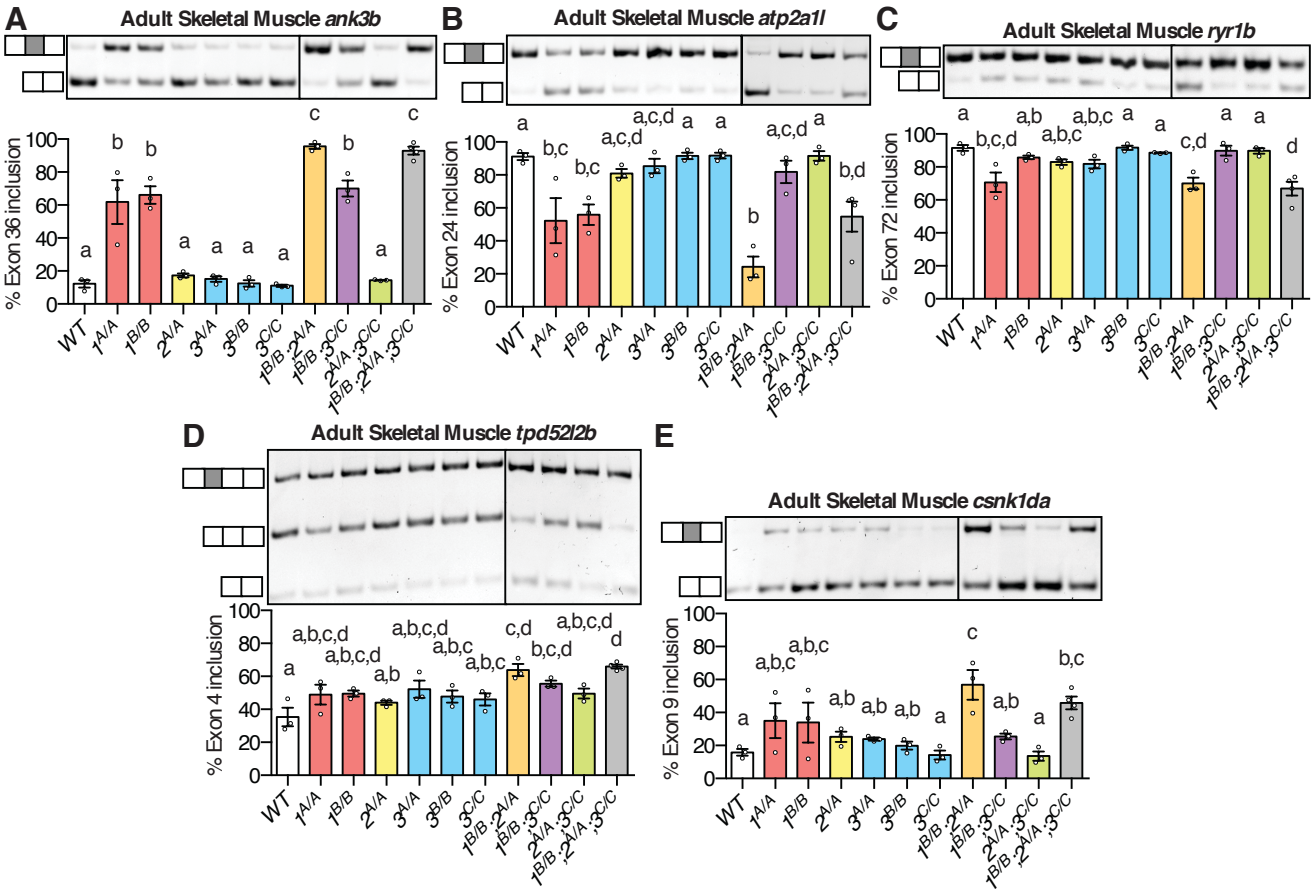

Figure 4 Misregulation of many myotonic dystrophy-associated alternative splicing events was conserved in zebrafish *mbnl* mutants. **A-E.** RT-PCR analysis showing inclusion of **(A)** *ank3b* exon 36, **(B)** *atp2a1l* exon 24, **(C)** *ryr1b* exon 72, **(D)** *tpd52l2b* exon 4, and **(E)** *csnk1da* exon 9 in WT and *mbnl* mutant adult zebrafish skeletal muscle. For all graphs, homozygous *mbnl1* mutant alleles are denoted as 1^A and 1^B, *mbnl2* alleles as 2^A, and *mbnl3* alleles as 3^A, 3^B, and 3^C. Each dot represents RNA from one fish. Error bars indicate standard error of the mean. Representative RT-PCR gels are shown above each graph. Dividing lines indicated samples run on separate gels. Data were analyzed by ordinary one-way ANOVA with Tukey's multiple comparisons test. Data bars that do not share a letter above them are significantly different from one another.

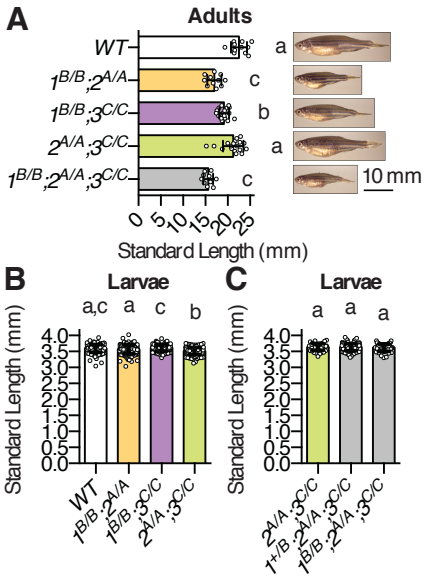

Figure 5 Double and triple homozygous *mbnl* mutant zebrafish were decreased in length. A. Standard length of young adult 60 days post fertilization (dpf) WT and *mbnl* mutant zebrafish that were raised in the same tank. On the right are representative images of fish of each genotype taken at 76 dpf. **B.** Standard length of 7 dpf WT and double *mbnl* mutant zebrafish. **C.** Standard length of 7 dpf clutchmates from an incross of *mbnl1*$^{+/B}$;*mbnl2*$^{A/A}$;*mbnl3*$^{C/C}$ fish. For all graphs, homozygous *mbnl1* mutant alleles are denoted as *1*^{A} and *1*^{B}, *mbnl2* alleles as *2*^{A}, and *mbnl3* alleles as *3*^{A}, *3*^{B}, and *3*^{C}. Each dot represents one fish and error bars indicate standard deviation. Data were analyzed by ordinary one-way ANOVA with Tukey's multiple comparisons test. Data bars that do not share a letter above them are significantly different from one another.

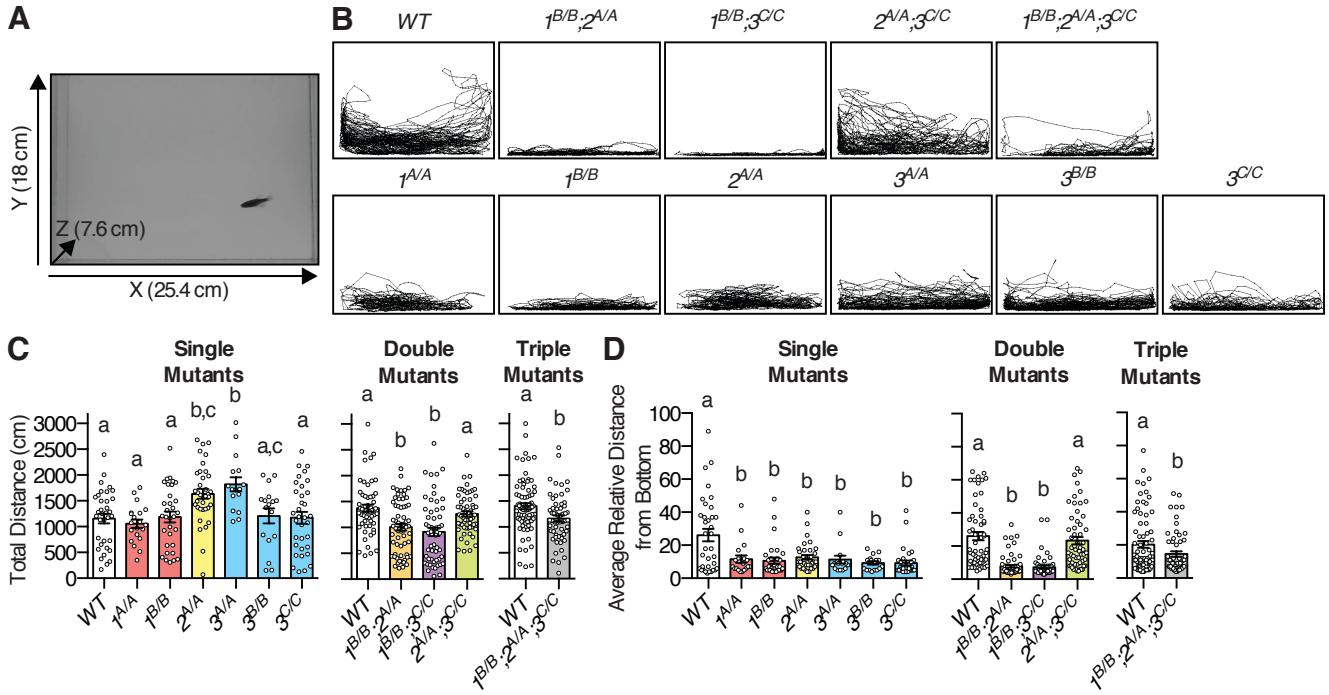

Figure 6 Zebrafish *mbnl* mutants exhibited altered swimming behavior. A. Example still image taken from video of swim tests. Software was used to track the center of mass of each fish in the X and Y directions over 5 minutes. **B**. Representative traces of individual fish of each genotype taken during the swim tests. X and Y axes are the same as in A. **C.** Total distance that adult fish swam during a five-minute swim test. The Y axes are the same for all three graphs. **D.** Average relative distance from the bottom of the tank of fish during a five-minute swim test. Zero represents the bottom of the tank and 100 represents the top of the tank. The Y axes are the same for all three graphs. For all sub-figures, homozygous *mbnl1* mutant alleles are denoted as 1^A and 1^B, *mbnl2* alleles as 2^A, and *mbnl3* alleles as 3^A, 3^B, and 3^C. Each dot represents one fish and error bars indicate standard error. Single and double mutant data were analyzed by ordinary one-way ANOVA with Tukey's multiple comparisons test, while triple mutant data were analyzed by a Student's t-test. Data bars that do not share a letter above them are significantly different from one another.